

The REM Telescope: Detecting the Near Infra-Red Counterparts of Gamma-Ray Bursts and the Prompt Behaviour of Their Optical Continuum

F.M.ZERBI¹, G.CHINCARINI^{1,2}, G.GHISELLINI¹, M.RODONÓ³, G. TOSTI⁴, L.A. ANTONELLI⁵, P. CONCONI¹, S. COVINO¹, G. CUTISPOTO³, E. MOLINARI¹, L. NICASTRO⁶, E. PALAZZI⁷, C. AKERLOF⁸, BURDERI⁵, S. CAMPANA¹, G. CRIMI¹, J. DANZINGER⁹, A. DI PAOLA⁵, A. FERNANDEZ-SOTO¹, F. FIORE⁵, F. FRONTERA¹⁰, D. FUGAZZA¹, G. GENTILE³, P. GOLDONI¹¹, G. ISRAEL⁵, B. JORDAN¹², D. LORENZETTI⁵, B. MC BREEN^{12,13}, E. MARTINETTI³, R. MAZZOLENI¹, N. MASETTI⁷, S. MESSINA³, E. MEURS¹³, A. MONFARDINI¹⁴, G. NUCCIARELLI⁴, M. ORLANDINI⁷, J. PAUL¹¹, E. PIAN⁹, P. SARACCO¹, S. SARDONE³, L. STELLA⁵, L. TAGLIAFERRI¹, M. TAVANI¹⁵, V. TESTA⁵, F. VITALI⁵

¹ INAF - Osservatorio Astronomico di Brera, Via Bianchi, 46, I-23807, Merate (Lc) Italy

² Università degli Studi Milano-Bicocca, Dipartimento di Fisica,

³ INAF - Osservatorio Astronomico di Catania, Via S.Sofia, 78 - I-95123 Catania - Italy

⁴ Università di Perugia, Dipartimento di Fisica, Piazza Università 1, I- 06100 Perugia, Italy

⁵ INAF - Osservatorio Astronomico di Roma, Via di Frascati, 33 I-00040 Monte Porzio Catone Italy

⁶ CNR-IFCAI, Via Ugo La Malfa 153, 90146 Palermo, Italy

⁷ CNR-TESRE, via P. Gobetti, 101 40129 Bologna, Italy

⁸ Randall Laboratory of Physics, 500 East University, Ann Arbor, MI 48109-1120, USA

⁹ INAF - Osservatorio Astronomico di Trieste, via Tiepolo, 11 - I-34131 Trieste - Italy

¹⁰ Università di Ferrara, Dipartimento di Ingegneria, Via Saragat 1, I-44100 Ferrara, Italy

¹¹ Service d'Astrophysique, CEA-Saclay, 91191 Gif sur Yvette, France

¹² DIAS - Dunsink Observatory, Castleknock, Dublin 15, Republic of Ireland

¹³ Univeristy College Dublin, Belfield, Dublin 4, Republic of Ireland

¹⁴ Univerit  di Trieste, Piazzale Europa, 1 I-34127 Trieste, Italy

¹⁵ CNR-IFC, via Bassini 15, I-20133 Milano

Received *date will be inserted by the editor*; accepted *date will be inserted by the editor*

Abstract. Observations of the prompt afterglow of Gamma Ray Burst events are unanimously considered of paramount importance for GRB science and related cosmology. Such observations at NIR wavelengths are even more promising allowing one to monitor high- z Ly- α absorbed bursts as well as events occurring in dusty star-forming regions. In these pages we present REM (Rapid Eye Mount), a fully robotized fast slewing telescope equipped with a high throughput NIR (Z, J, H, K) camera dedicated to detecting the prompt IR afterglow. REM can discover objects at extremely high redshift and trigger large telescopes to observe them. The REM telescope will simultaneously feed ROSS (REM Optical Slitless spectrograph) via a dichroic. ROSS will intensively monitor the prompt optical continuum of GRB afterglows. The synergy between REM-IR cam and ROSS makes REM a powerful observing tool for any kind of fast transient phenomena.

Key words: cosmology:observations, instrument:miscellaneous, gamma rays, infrared radiation

1. Introduction

REM (Rapid Eye Mount) is a fully robotic fast-slewing telescope primarily designed to follow the early phases of the afterglow of Gamma Ray Bursts (GRB) detected by Spaceborne γ -alert systems such as HETE II, INTEGRAL AGILE, Swift. REM is currently under construction and will be installed at la Silla Observatory Chile, in the framework of the Fast Robotic Observatory System for Transients (FROST) collaboration, formed by the REM/ROSS team and the TAROT-S team. TAROT-S (see Boer et al, these proceed-

ings) is a fast optical imager that will provide coordinates of optical transients with sub-arcsec precision on time-scales of a few seconds upon trigger reception. TAROT-S is in this sense complementary to REM/ROSS.

REM has been conceived to host a NIR (Near Infra-Red) camera covering the 0.95-2.3 μm range with 4 filters (Z,J,H,K). In a second phase of the project it has been decided to host ROSS (REM Optical Slitless Spectrograph), a slitless spectrograph covering the range 0.45-0.95 μm with 30 sample points, originally conceived as a stand alone telescope/instrument. As a consequence REM will serve as

a Rapid-pointing broad band spectro-photometric facility whenever prompt multi-wavelength data are needed.

REM is a very ambitious project since it can lead to the discovery and study of the most distant astronomical sources ever observed so-far. It is known that roughly a half of the GRBs observed so far do not show any optical afterglow. At least a part of them can be high- z bursts for which Ly- α absorption dumps all the light at optical wavelengths. Ly- α absorption falls in the REM wavelength range for sources with red-shift between 8 and 15, i.e. any burst in this range can still be detected by REM and its position determined with an accuracy of a few tenth of arcsec. The Astrometry will be made available on a time-scale of tens of second allowing one to observe the transient with larger area telescopes when it is still very bright.

Via REM a 8-mt class telescope equipped with suitable IR spectrographs, could collect a high resolution high S/N spectrum of a source at $z \gtrsim 10$, i.e. the most distance source within or beyond the range of the expected red-shift of re-ionization ($8 < z < 20$). ROSS is as well an outstanding instrument since it will intensively monitor the shape of the optical afterglow continuum and its early temporal behaviour. ROSS will allow to constrain the models for the prompt afterglow emission and will provide, together with REM-IR camera, useful information about GRB progenitors and GRB environments.

2. Scientific Rationale

Gamma Ray Bursts are bright, transient events in the γ -ray sky, unpredictable in time and location, with a typical duration of the order of seconds. The brightest bursts have γ -ray fluences (flux integrated over the time for its duration) of $\sim 10^{-4}$ erg cm $^{-2}$. Most of the energy is released in the 0.1-1 MeV range. Spectra generally display featureless smooth continua.

After 30 years since their detection by the VELA satellites, we now start to understand the physics of GRBs. This has been made possible by the precise location of the Wide Field Camera (WFC) of Beppo-SAX, which allowed the detection of their X-ray afterglow emission (Costa et al. 1997) and the optical follow up observations, leading to the discovery that they are cosmological sources (van Paradijs et al. 1997). The huge energy and power release required by their cosmological distances support the fireball scenario (Cavallo & Rees 1978; Rees & Meszaros 1992; Meszaros & Rees 1993), even if we do not know yet which kind of progenitor causes the GRB phenomenon.

The most accepted picture for the burst and afterglow emission is the internal/external shock scenario (Rees & Meszaros 1992; Rees & Meszaros 1994; Sari & Piran 1997). According to this model, the burst emission is due to collisions of pairs of relativistic shells (internal shocks), while the afterglow is generated by the shocks produced by shells interacting with the interstellar medium (ISM, external shocks).

The emission mechanism operating during the burst proper is still an open problem: synchrotron (Rees & Meszaros 1994; Sari, Narayan & Piran 1996), quasi thermal Comptonization (Liang 1997; Ghisellini & Celotti 1999) and

Compton drag (Lazzati et al. 2000) have all been proposed. For the afterglow there is instead strong evidence that the main radiation mechanism is the synchrotron process, since this well explains the power law decay of the flux with time, the observed power law energy spectra and the detected linear optical polarization in GRB 990510 (Covino et al. 1999, Wijers et al. 1999) and in GRB 990712 (Rol et al 2000). The afterglow emission is believed to be due to the interaction of the fireball with the circum-burst material, when enough ambient matter is swept up by the fire-ball.

The resulting shocked material is accelerated to random ultra-relativistic energies in an amplified magnetic field, and radiates by the synchrotron process. Two shocks develop: a forward shock thought to be responsible for most of the afterglow light in all bands, and a reverse shock, thought to be responsible for the initial emission in the IR-UV band, called the optical flash.

For about 20 GRBs we have a spectroscopic estimates of the redshift (updated September 2001). In the case of GRB 980329 an estimate was based on the cut-off in the spectrum interpreted as Ly- α absorption by Fruchter (1999). GRB 980425 is instead identified with the supernova SN1998bw. For those bursts of known distance, we can calculate the energy emitted during the burst: the energy ranges between 10^{51} and 10^{54} ergs i.e., assuming isotropic emission, of the order of one solar mass entirely converted into energy.

When an afterglow is detected the monochromatic flux decreases in time as a power law $F_\nu(t) \sim t^{-\delta}$ with δ in the range 0.8-2. Usually, the magnitudes of the optical afterglow detected about one day after the γ -ray event are in the range 19-21. It has been suggested that the steepest observed light curves are the result of beaming. According to this idea, the decay index $\delta \sim 1$ at early times and after a few hours steepens to $\delta \sim 1.5 - 2.0$. Assuming $m=19$ after 24 hours and $\delta \sim 1.5$, the expected magnitude after 1 hour is ~ 13.8 . GRB 990123 has been detected by the robotic telescope ROTSE 22 seconds after the γ -ray trigger at $m \sim 11.7$, reaching $m \sim 8.9$ 47 seconds after the trigger (Akerlof & McKay 1999).

Many fascinating questions remain open about GRB origin and structure. Some of these questions should be answered by collecting data in the early phases of the afterglow. For these reasons the international astronomical community developed space borne observatories dedicated entirely (HETE II, Swift) or partly (AGILE, INTEGRAL) to detect and send promptly a trigger with the position of the GRB to ground-based follow-up facilities. the aim of these facilities is to record in a timely manner relevant information and act as an inter-mediate step to activate Target of Opportunity procedure at telescopes with larger area. A fast response automatic facility is then highly desirable. REM is one of these, the only one foreseen so far to monitor the near infrared region as well as to sample intensively the optical continuum.

2.1. REM and GRBs

Although we have only one example of prompt optical/IR emission during the first minutes of the afterglow (GRB

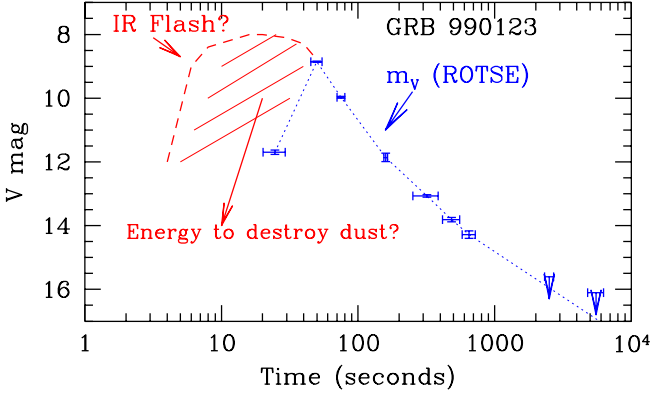


Fig. 1. The optical flash of GRB 990123 as seen by ROTSE. Part of the optical/UV photons could have been absorbed by dust, in the first part of the emission. After dust has evaporated, the line of sight become extinction free. Since IR photons are much less absorbed by dust, they could pass nearly unabsorbed, resulting in a more prompt emission.

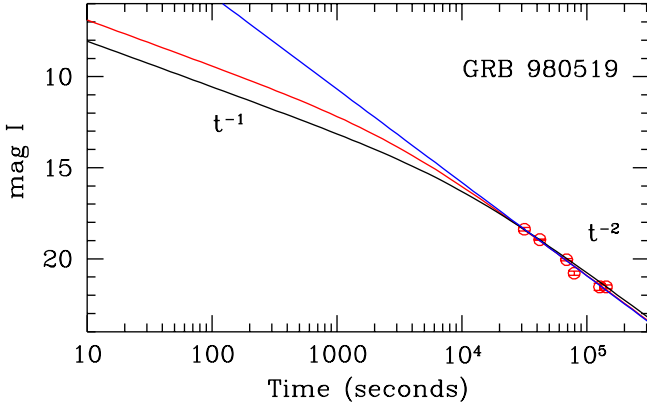


Fig. 2. The optical light curve of GRB 980519, with 3 possible extrapolation towards earlier times. Should the early afterglow behave normally (i.e. with a t^{-1}) we would have evidence of beaming

990123, figure 1), we can estimate the typical early magnitudes by extrapolating back in time the light curves of known afterglows, as shown in figure 2 and figure 3. From the instruments description reported below we can see that the REM telescope with its NIR camera is expected to reach magnitude $H=15.5$, 16.04 and 17.11 with exposure times of 5, 30 and 600 seconds respectively ($S/N=5$). With the ROSS spectrograph (see figures 11 and 12) a $V=14$ point-like source is recorded better than 10σ in 1 sec exposures.

The above numbers suggest that we can detect the IR afterglow during the first 2-4 hours even with an exposure time of 5 seconds. This will allow the study of the light curve and eventual flickering in great detail, the detection of possible (even if short) variations from the smooth power-law behavior and the definition of any possible break. Increasing the exposure time (after the initial phases) to 10 minutes, we can follow typical bursts up to 12 hours, after which larger telescopes can take over. We give below a brief description of the key points that REM can address concerning GRBs.

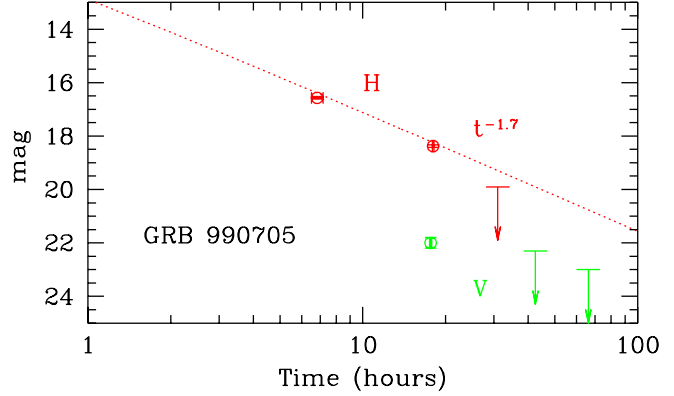


Fig. 3. The Infrared (Hband) light curve of GRB 990705, with a possible extrapolation towards earlier times. Also shown is the only detection point in the Vband (green point). The estimated V-H color is 3.5-4, suggesting either a steep continuum or strong reddening.

2.1.1. High-z Bursts

If a burst is at high- z , $Ly-\alpha$ absorption dumps all the light at optical wavelengths. $Ly-\alpha$ absorption falls in the REM NIR camera wavelength range for sources with red-shift between 8 and 15, i.e. any burst in this range can still be detected by REM NIR camera and its position determined with an accuracy of a few tenths of an arcsec. The simultaneous detection in the IR and a non-detection in the optical can directly flag the presence of a high- z object.

A highly absorbed burst might as well dump the optical photons out but the color-color techniques can discriminate between the two possibilities and select good candidates high- z objects automatically and in real time. Large telescopes (such as VLT) can then point at the target while it is still bright enough for high-dispersion spectroscopic observations. This appears to be the only way to obtain high quality spectra for large redshift (even $z > 10$) objects, to study the distribution of $Ly-\alpha$ clouds with redshift, their metallicity etc. Moreover, in the majority of cases, GRBs are associated with galaxies. The detection of a very high redshift GRB would hence mark the likely location of a very high redshift galaxy.

When REM will be operated with Swift the information of the non detection of an optical transient will be promptly made available by the UVOT monitor on-board the satellite. When operated with other trigger systems, however, the collaboration with TAROT-S in the framework of the FROST Collaboration will be of paramount importance.

2.1.2. Reddened Bursts

If the burst is not at high redshift the absence of an optical afterglow can be due to absorption by intervening matter (dust), either in the close vicinity of the burst (if exploded in a dense star forming region whose dust has not been completely destroyed by the burst emission itself), or by dust distributed along the line of sight, even at large distances from the burst site. In this case the infrared light is much less absorbed, and therefore an IR transient can be detected even if the optical

is not. From this point of view, the REM telescope, combining the two (IR and optical) datasets, will make possible to estimate the amount of absorption.

The above is important since a lack of dust absorption, thought to be associated with star-forming regions, has been reported in the spectra of bursts. A possible explanation for such a lack is that dust grains are sublimated by the prompt optical/UV emission (see above and Fig. 1). In this case, an *IR flash* should be observed to start before the optical one, as the IR radiation can penetrate unabsorbed in the cloud while the higher energy photons progressively clean out the dust. The observed IR fluence before the detection of the optical flash would greatly constrain the amount of dust in the cloud.

2.1.3. Broad Band Spectrum

Even if the theory of afterglow emission (due to synchrotron) is largely accepted, the best constraints we have come from observations performed one or several days after the GRB. In fact, the polarization was observed ~ 1 day after the explosion, and, for example, the broad band spectrum of GRB 970508 has been measured 12 days after the γ -ray trigger. It is however possible (if not even likely) that at the beginning of the afterglow the physical conditions (density and temperature) of the shocked material are more extreme and that different emission processes (e.g. Comptonization) are dominant. A non-uniform ISM distribution (e.g. a wind r^{-2} profile) would strengthen these differences even more. Increasing the "frequency leverage" is therefore of great importance to better determine the spectrum of the early afterglow. The available information from a good quality spectrum is a test of the afterglow emission process, a constraint of the ISM distribution (and hence gives insight for the problem of the progenitor) and is a measure of the optical extinction.

2.1.4. Same Co-moving light curve

If bursts with different redshifts are observed at the same wavelength, a comparative analysis is hardly possible since the rest frame wavelength of the observations is different. If, however, multifilter observations are systematically performed for all bursts, it is possible to compare between them magnitudes (or fluxes, spectra) at the same comoving frequency. The larger the spectral baseline of the observations, the larger set of redshifts can be consistently compared. The wide spectral range covered by REM-IR camera and ROSS spectrograph allows the comparison in an unprecedented wide range of redshifts.

2.2. Additional Science Program

The REM telescope, as all other robotic facilities dedicated to GRB science, reacts to a trigger from a space-borne satellite. This means that for a considerable amount of time REM will be idle in the sense that it will not be pointing at any GRB transient. Such a time depends on the number of public triggers eventually provided by missions scheduled to fly during REM operation is estimated to be around 40% of total REM observing time. During the idle phase REM will serve the

community as a fast pointing NIR imager and optical spectrograph particularly suitable for multi-frequency monitoring of highly variable and transient sources.

Among the obvious applications of REM idle time there are AGN and variable star multi-frequency monitoring. Some Key-programs of interest have been already identified by the REM science team and the related preparatory work has been initiated. REM will be used in association with INTEGRAL to monitor Galactic Black Hole candidates flare stars and with AGILE for Blazar monitoring.

2.2.1. Galactic Black Holes Candidates

To obtain a complete picture of accreting binary systems, near infrared and optical observations can be fundamental as they allow one to estimate the compact object mass through mass function measurements. Indeed this is the best method available to establish the real nature of Black Hole Candidates (BHCs) identified at other wavelengths (usually X-rays). Even if this measure is not always possible, other measurements of e.g. the spectral type of the companion star are of great help in understanding the accretion phenomenon and the evolutionary history of the system. Near Infrared (NIR) observations are better suited to this research than optical ones as they suffer less from contamination from the accretion disk and galactic absorption. Optical data can instead help in the determination of the spectral type of the companion.

Of particular importance in this field are the observations of X-ray Novae (Tanaka & Shibazaki 1996), this class of transient in fact contains the majority (11 of 14) of BHCs with dynamically measured mass functions (Tanaka & Shibazaki 1996, Filippenko et al. 1999, Mc Clintock et al. 2001, Orosz et al. 2001). These sources are discovered during an outburst during which they first become very bright, then progressively less luminous and in the end almost undetectable. Their X-ray emission evolves into different spectral states which probably correspond to different mass accretion rates. Most of all, at the end of the outburst X-ray emission becomes so faint that it is possible to measure the optical mass function of the system and hence the BH Mass. X-ray Novae offer therefore an ideal test case for the study of accretion processes in Black Holes. Several phenomena at different wavelengths (radio jet emission, optical/NIR brightening...) are often visible during the X-ray Nova outburst.

To properly characterize the outburst mechanism and the succession of events, a fast identification of the optical counterpart is essential in order to allow a continuous monitoring parallel to X-ray results. Given the relatively bright magnitudes of these objects ($V \sim 13$ at maximum for Nova Muscae 1991 (Della Valle et al. 1991)) and the error box that can be provided by present-day X γ -ray instruments (less than 1 arcminute), REM can easily perform the identification and follow the light curve with multicolor photometry (and slitless spectroscopy) while high signal to noise spectra could be obtained with larger telescopes.

2.2.2. Blazars

Blazars are the most violent subclass of active galactic nuclei, emitting across the entire electromagnetic spectrum, and being characterized by large amplitude variability in short time-scales (factor 2 in hours, factor 100 in weeks/months). Blazars are important because their emission is produced by plasma flowing at relativistic speeds through jets, from the very inner core of the nucleus (i.e. a few Schwarzschild radii) to distances as great as hundreds of Kpc.

The spectral energy distribution (SED) of Blazars is characterized by two broad peaks: the first is in the IRUV band, the second the MeV-GeV band. There is unanimous consensus that the first broad peak is due to synchrotron emission, while the nature of the second peak is still under discussion. Most likely, it is due to the inverse Compton process by the same electrons producing the synchrotron photons.

Recent multiwavelength observing campaigns seem to find that a coordinated variability at different frequency bands is present in Blazars. This would mean that the two peaks of emission are caused by the same population of electrons at the same location of the jet and that there is a localized region, in the jet, where most of the radiation is produced. The same campaigns point out that at frequencies lower than the peak the variability is less violent.

This could be due to a difference in cooling times between the electrons producing the higher frequency and the lower frequency flux. It could be also due to a different dimension of the portion of the jet corresponding with the flux formation in the sense that the flux at lower frequencies is produced in a more extended part of the jet. The way to discriminate between these two options is dense monitoring at frequencies below and above the synchrotron peak, to search for any possible time lag (which would favor the first hypothesis) or simultaneous variations of decreasing amplitude for decreasing frequencies (which would favor the second hypothesis).

Blazars are classified according to the presence or absence of strong emission lines and according to the location of the synchrotron peak. Fossati et al. (1998) and Ghisellini et al. (1998) showed that the different behaviour depends mainly on the bolometric luminosity of the source. For instance Blazars peaking in the near infrared are the subclass of the classical BL Lacs and FSRQs discovered through radio means. We then expect that the IR spectrum for these sources is characterized by a power law of index ~ 1 : $F(\nu) \propto \nu^{-1}$. Steeper spectra are expected for more powerful sources (having their synchrotron peak at even lower frequencies), and flatter spectra for lower luminosity BL Lacs.

The limiting sensitivity of REM-IR camera and ROSS spectrograph allows one to observe about 2/3 of all known blazars (i.e. around 300 objects). This means that there will be plenty of possible candidates for observations with REM. In addition, since REM will be operational at the same time as AGILE (sensitive between 0.05 and 30 GeV), simultaneous observing campaigns can be organized, or prompt ToO REM observations performed in response to particularly intense flaring γ -ray states of some Blazars.

2.2.3. Flare Stars

Flare stars may produce γ -ray fluxes of the same order as GRBs. Flare events occur in the atmospheres of several types of stars, from pre-MS to post-MS cool stars and involve the entire stellar atmosphere, from the photosphere up to coronal layers. Owing to the rather different physical characteristics of these different layers, with temperatures and densities spanning several decades, the flare occurs in a wide range of wavelengths, from microwaves to X-rays, and possibly γ -rays as on the Sun: a striking example of a fast multi-wavelength phenomenon that requires really simultaneous observations in different bands.

A flare is generally characterized by an unpredictable flux increase of the order of up to 100 times the quiescent flux in a typical time scale of the order of 10-100 s. Then the flux decreases to the pre-flare level on time scales 10-100 times longer (see Rodonó 1990). The possibility of observing γ -ray emission from stellar flares has been predicted, among others, by Becker & Morrison (1974). Multi-wavelength studies (Rodonó & Cutispoto 1988; Rodonó et al. 1989) have shown that on the occasion of intense flares, with enhanced microwave, UV and optical flux increase, the IR flux decreases by a few percent. Such "negative" flares are predicted by a non-thermal model based on the inverse Compton process (Gurzadian 1977) and a thermal model based on the increased opacity of the negative H ion (Grinin 1976).

However, owing to the paucity of the observed events, no conclusion about their nature can be drawn. What is impressive is that the missing energy in the K-band alone can account for the energy flux increase at all other wavelengths. Relatively small "negative" flares or flare "dips" are sometimes observed close to the occurrence of some flares (Rodonó et al. 1979, Cristaldi et al. 1980).

2.2.4. Serendipity and Targeted Observations

In addition to primary and secondary targets a number of by-products are expected from REM observations. These are serendipitous discoveries of variable objects falling in the transients field and precise determinations of NIR colors and continuum shape of any object falling in the same fields.

The processing and storage of these serendipitous data will be done off-line and based on the storage media transported to the REM European Headquarters. There instrumental magnitudes will be computed and converted into standard colors. There as well the correlation between images (and spectra) collected at different epochs will allow one to disentangle variable phenomena and, if the case analyze their characteristics. All the data will be made public in a short time in a data base accessible via the internet.

A limited amount of time will also be available for individual proposals. The handling of this time will be taken care of by the REM science team which will receive, process, accept or refuse the proposal. The REM team will then define the procedure and scheduling of such individual observations and provide the applicant with the data.

3. The REM telescope

The REM telescope is a Ritchey-Chretien system with a 60 cm f/2.2 primary and a overall f/8 focal ratio mounted in an alt-azimuth mount in order to provide stable Nasmyth focal stations, suitable for fast motions. REM has two Nasmyth focal stations although at first light one will remain idle. At the first focal station a dichroic, working at 45 degrees in the f/8 convergent beam, will split the beam to feed the two first light instruments of the REM telescope: the REM-IR camera and the ROSS Spectrograph. The mirrors are made by Zeiss and they are coated with protected silver to maximize reflection efficiency in such a large (0.45 - 2.3 μ) wavelength range.

The dichroic, a crucial element, has been designed in house with the aim to achieve the maximum possible transmission at IR wavelengths (0.95-2.3 μ m) and the maximum possible reflection at Optical wavelength (0.45-0.95 μ m). Unavoidable losses will occur in the transition region, i.e the region in which the efficiency of both transmission and reflection drops. Care has been then taken to define where the cut should be positioned according to the scientific requirements and according to the response at shorter and longer wavelengths of the visible and the IR detector. The solution adopted provides a cut at 0.95 μ m and is made of a multi-layer coating of MgF_2 and ZnSe on a substrate of IR-SiO_2 . The transmission curve of the dichroic is given in figure 8.

The reflectivity reported in figure 8 is the average between that computed at 42° e 48° . The transmission of the device is strictly complementary to the reflectivity since the materials used have negligible absorption. The average reflectivity between 0.45 and 0.90 μ m is 0.965 with a minimum of 0.880. The average transmission between 1 and 2.3 μ m is 0.972 with a minimum of 0.91. There is obviously a polarizing effect (the curves are the mean of the S and P components) that will have to be calibrated once the device is mounted at the telescope.

The REM telescope is currently being manufactured by Halfmann Teleskoptechnik GmbH (HT) in Neusäß (Augsburg, BRD). HT has expertise in the field of professional astronomical instrumentation. Engineers from HT actively took part in the design phase of the telescope suggesting the solution best suitable to our requirements. A schematic layout of the telescope mechanics is reported in figure 4

3.1. Telescope Control and Operation

The robotic character of the REM telescope and the minimization of the need for human intervention is mainly obtained via a robust operation scheme and a highly modular and reliable operation software. The main aim that drives the project is to deliver a system able to take decisions in a few seconds without any human intervention. However, an adequate interface to allow a remote human control of operations in case of necessity is developed. In principle, our system can be subdivided from a logical point of view in several subsystems that manage the various duties of the experiment: the REM Observing Software (REMOS), the REM Telescope Control System (REMTCS), the REM Camera Control Software (REMCCS), the REM Dome Control Software (REMDCS), the REM Environmental Control Software

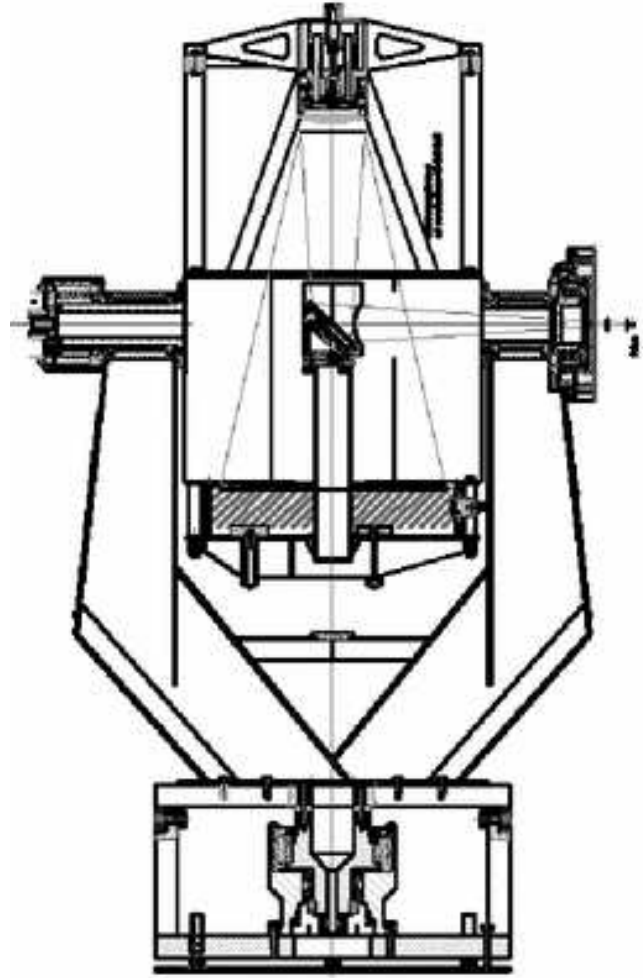


Fig. 4. Schematic overview of the telescope mechanics. Courtesy of Teleskoptechnik Halfmann.

(ECS) and the ROSS spectrograph control software. All these subsystems can work on different or common CPUs, depending on the specific needs. A certain degree of redundancy is foreseen.

The most general working scenario starts with the reception by an efficient socket connection of an alert message from the GCN (<http://gcn.gsfc.nasa.gov/gcn/>). The message announces the detection of a GRB. Now, the REMOS checks if the possible target satisfies some minimum visibility constraints (hour angle, altitude, Sun and Moon distance, etc.). If these conditions are verified, information from REMECS is retrieved and if observations are possible (humidity, wind, sun altitude, etc., within safety and operational limits) REMOS checks if the system is already busy with observations of a different target. If this is the case, and the source is another GRB, a decisional algorithm is applied. Depending on the specific case (Infrared Transient, IT, already discovered, γ -ray fluence, favorable sky position, time interval from the GRB, etc.) eventually a decision is taken. In the positive case (new GRB to be observed) or in case the telescope was observing some lower priority target, REMOS sends a message via socket connection the REMTCS stopping operations and moving the telescope to the new target. As soon as the

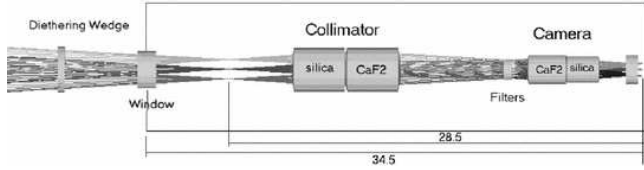


Fig. 5. REM-IR camera design. The camera is a focal reducer (F/8- F/5.3) with separated doublets for collimator and camera. A cold stop is inserted for background reduction where the pupil is reformed: the filters are as well inserted in the collimated beam. In front of the cryostat window we find the rotating plate used for dithering

REMTCS communicates that the telescope is on target the REMOS sends messages to the REMCCS and ROSS to begin observations with some predefined templates. Immediately after the first frames are obtained, they are analyzed by the REM Reduction Software (REMRS) that can, if necessary, send new coordinates to the REMOS, i.e. to better center the target, or modify the observing templates, i.e. in case of peculiarly bright or faint IT.

Of course the REMOS also periodically samples the environmental conditions in order to drive the opening or closing of the dome by the REMDCS and stops operation in case some safety alarm is triggered (un-expected intrusion in dome, etc.). Apart from the reaction to a GRB alert, it is possible by a web based interface to provide the telescope coordinate list and observing parameters for any target to be observed for the additional science programs. These operations follow basically the same outline, even if any new low priority target is observed only after the completion of all operations on the previous one on the priority list. It is also possible to prepare observations of a target on a specific schedule, i.e. for simultaneous observations, or under specific observing conditions, i.e. zenith distance.

4. The REM-IR Camera

The REM camera follows a focal reducer design in order to reform a white pupil in a cold environment for Lyot-stop positioning (see figure 5). A filter wheel with 10 positions is located at the reformed pupil allowing one to insert filters and grisms for slit-less spectroscopy or polarimeters in a parallel beam. The camera changes the focal ratio from f/8 to f/5.3 providing a plate-scale of 64.4 as/mm that allows one to position a $9.9 \times 9.9 \text{ arcmin}^2$ FOV on a 512×512 ($18 \mu\text{m}$ pitch) HgCdTe chip in production at Rockwell. Both collimator and camera are made of a Silica-CaF₂ doublet (the latter reverse-mounted). The total thickness of the optical design is 300 mm. The image quality is optimal as can be seen in the spot diagrams reported in figure 6

The whole camera train is mounted in a dewar and operated in a cool environment. The chip working temperature is 77 K and will be guaranteed at the detector location and at the cold stop position. The optical train is kept at a temperature of about 100-120 K in order to save cooling power. The cryogenics are supported by a Stirling-Cycle cryo-pump

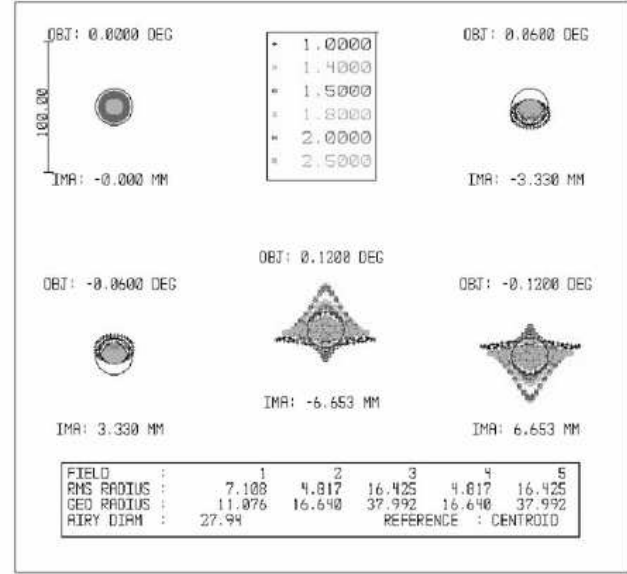


Fig. 6. Polychromatic (1.0 - 2.5 μm) spot diagrams for REM-IR Camera. The bold circle represent the diffraction limit which is reached almost at any field.

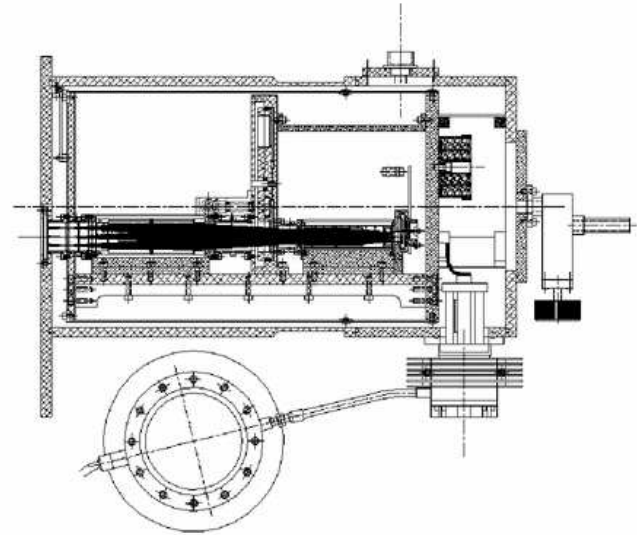


Fig. 7. Mechanical layout of the REM-IR Camera. The optics are mounted in slightly decentered vacuum dewar. The detector, the cold stop and the inner lenses are cooled via a closed circuit Stirling Cryo-pump. Drawing courtesy of IR-Labs, Arizona

requiring limited maintenance and no need for dewar refilling. A sketch of the mechanical layout of REM-IR camera is shown in figure 7.

The REM-IR camera needs dithering of the images for noise reduction and sky subtraction. However such a dithering can not be provided moving the telescope since the ROSS spectrograph needs a stable image for longer integrations. The dithering will then be provided by a plate with plane parallel surfaces inserted with a given tilt (18°) in front of the cryostat window, i.e. after the dichroic. The effect of the plate is to translate the image of 20 pixels from the nominal

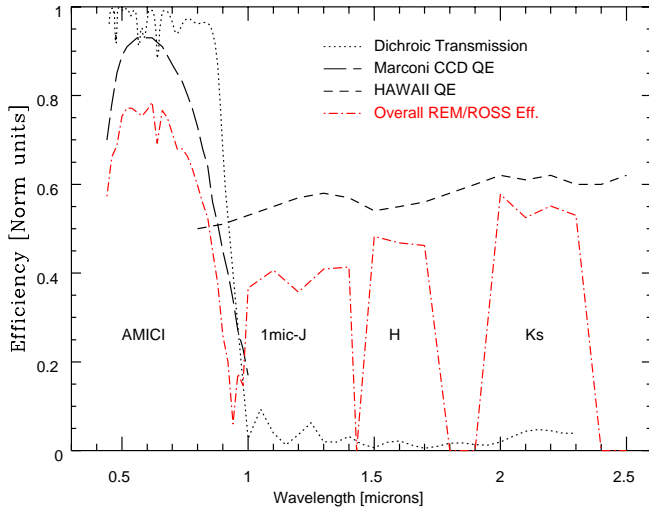


Fig. 8. Overall Efficiency of the REM IR camera and ROSS. We show in the plot the transmission of the dichroic, the QE of the Marconi CCD and of the HAWAII Chip and an estimate of the "all-included" efficiency of the instruments.

position (no plate inserted) along a given direction. By rotating the plate in the beam such a direction and hence the displacement of the image can be changed at will providing the dithering. A rotary stage changes the orientation of the plate, the angle is read by an encoder and transmitted to the Reduction software making the image reconstruction possible.

By taking into account glass transmission and reflection (with suitable AR coating) the overall transmission of the camera (telescope, array and filters not included) is estimated to be about 85%. An additional 2% loss should be expected from the Telescope (silver coated) and the minimum expected transmission of the dichroic (see above) is 91%. HAWAII chips have peak efficiency around 64% while from 0.9 to 2.5 μm it is never lower than 56%. Therefore we should expect an overall efficiency of about 59% (43% minimum; filters excluded). The overall efficiency of the REM-IR camera is reported in figure 8

The regime in which REM-IR is operated is mainly sky limited and RON and DARK have little effect on the performance. We computed the limiting magnitudes using the usual formula for S/N calculations and NTT-SOFI J,H and Ks filters as a template for REM filters still under procurement. We assume the following average transmissions: 75%, 80% and 85% for J,H,K respectively. No predictions have been made for the Z filter since its transmission will be modulated a posteriori on the cut-on of the HgCdTe chip and the dichroic. The limiting magnitudes computed using these figures are reported in table 1.

The REM selected FOV has been selected to match the typical error-boxes of γ -ray alert systems. The need of absolute photometric measurements (magnitudes and IR color indices) makes the presence in the FOV of a number of comparison non-variable stars necessary. Simulation using the USNO-A1.0 Catalogue of objects from digitized plates have been performed. Using the server at the ESO/ST-ECF

Table 1. Limiting magnitudes as a function of the S/N (10 or 5) and of the passband, for the different integration times foreseen in the REM target operation.

T int.	J 10 σ	J 5 σ	H 10 σ	H 5 σ	K 10 σ	K 5 σ
5 sec	15.5	16.3	14.3	15.1	13.1	13.9
30 sec	16.4	17.2	15.2	16.0	14.1	14.8
600 sec	17.3	18.0	16.3	17.1	15.4	16.1

Archive an automated procedure retrieves a star chart showing the magnitudes and V-R colors of the stars. Targets are of random fields or for a given coordinates. Random fields are used to build a luminosity function in the FOV and preliminary results for the search of R=15 stars ranges from null detection to several dozen of objects. Part of the idle time of the REM telescope (i.e. on clear nights when the satellite is pointing to a forbidden, below horizon area) will be partly devoted to post-calibration of observed fields.

4.1. The Automatic Quick-Analysis Software

The Automatic Quick-Analysis software (AQuA) has been developed and entirely dedicated to the REM data using criteria of high speed, system stability and reliable results in a fully automated way. It will run on a high performance computer with double processor completely dedicated to data handling in order to find transient coordinates and colors. Time sensitive data are quickly distributed via internet to the recipients entitled to receive them (including ToO procedure at larger telescopes) while the bulk of data (2.5 Gbytes of data per night expected) is recorded in a portable storage system. In this scheme the only human intervention needed during normal operation is to change such a removable science team approximately once every 10 days.

Given the intrinsic rapidity of the phenomena rapid photometry is as essential as the rapid mount drive. Based on a flux model which evolves as $f \sim t^{-\delta}$ with $0.8 < \delta < 2.0$ we reckon that a measurement of each filter Z', J, H and K every 5 seconds in the first observations after targeting is the minimum acceptable frequency. Slower data flow will be allowed after a 1.5 minutes and a measurement every 30 seconds will be delivered. One hour after the trigger signal the frequency will be definitely slowed down to one measure every 10 minutes. We judge that, focussing on targets with a typical known visual (V) magnitude between 9 and 15, the system response is within scientific specifications if no abrupt changes in the spectral energy distribution show up.

The system is normally working on secondary science activity and waiting for a trigger from the camera acquiring system. When the trigger arrives the system is ready to receive FITS files from the camera directly on a shared disk. It has no command duty with the exception of a line open with the camera control to refine exposure parameters and provide refined coordinates. When the telescope starts to acquire the target the data analysis system will be alerted and it will wait

for the first set of images. As the first set of five dithered images will be available on the disk they will be preprocessed in order to obtain one scientific image corrected for bad pixels, flat and sky subtracted. As soon as the final image is ready it will be analyzed by a source detection algorithm and a list of targets will be extracted. Source positions will be compared with catalogues to both perform astrometry and look for possible candidates. In the following step photometry will be performed on the field and calibrated with 2MASS sources (if present in the field) or using instrumental characteristic (e.g. exposure time vs limiting magnitude). AQuA has been prepared and optimized in order to perform all these operations in few seconds, about the same time needed for the acquiring system to collect another set of images. When a second scientific image becomes available a second source list will be extracted and compared with the previous one looking for variable sources. Furthermore the two images will be subtracted and filtered and the resulting image will be inspected with the detection algorithm and results compared with the previous results. If any source is present in the field the Automatic Quik-Analysis Software will provide the Observation Software with a warning and a higher exposure time. On the contrary if a transient source will be found the AQuA will provide the OSW with the coordinates. Coordinates will be then delivered in an automatic way via e-mail to already existent Alert Networks (e.g. GCN) and/or to a dedicated mailing list (e.g. REM Alert Mail). As soon as positions from the SWIFT optical monitor will be delivered AQuA will cross check them with REM positions. If an IR transient is found but no optical transient is present in the field, AQuA will activate a ToO to the VLT providing it with transient coordinates. Once the IR source has been found the OSW will change the filter and AQuA will perform the analysis on the other images collecting magnitudes in different bands and performing color measures.

Consequently when operated in the Primary science mode, i.e. following GRB triggers, REM will produce 3 classes of output on different time-scales: the coordinate of the IR transient will be available in a few seconds; magnitudes and colors will be available in a few minutes (possibly giving a rough estimate of the distance of the burst via the photometric red-shift technique); light and color curves will be accurately computed off-line by an extended version of AQuA. Coordinates and colors, especially in the case of a high-redshift burst, are probably the most valuable science output REM can provide.

5. The ROSS Spectrograph

With an orthogonal development relative to the REM-IR camera optical axis REM Nasmyth A will accommodate the slitless spectrograph ROSS. The spectrograph consists of a fore optics which images a pupil at the location of the dispersing element and re-maps the focal plane onto the detector unit. The selected detector head is a commercial Apogee AP47 camera hosting a Marconi 47-10 1K x 1K 13 μm pitch CCD. The plate scale of the REM telescope (43 arcsec/mm) matches properly with the specifications and allows one to

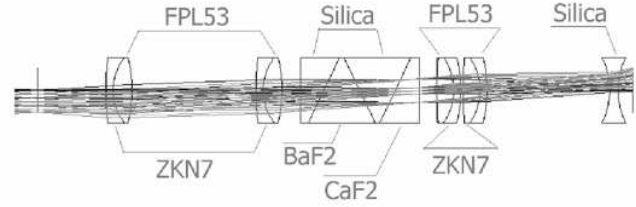


Fig. 9. ROSS Optical Layout. ROSS has a focal reducer scheme to reform a pupil to accommodate the AMICI prism. The natural scale of the telescope is however well suited for this instrument: ROSS works at magnification 1

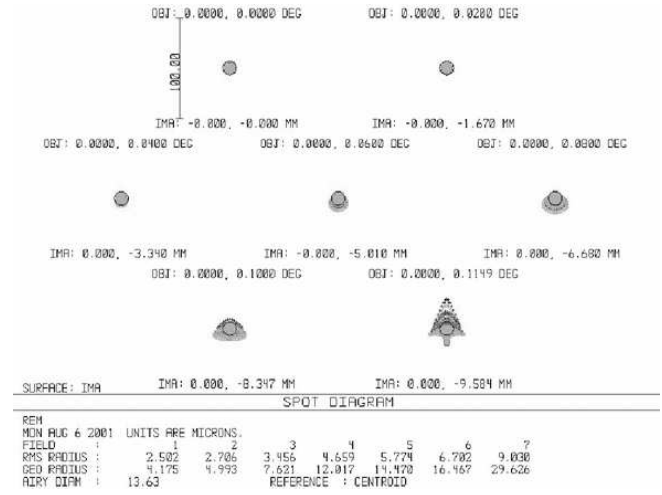


Fig. 10. ROSS Spot Diagram (with no AMICI inserted in the beam). The bold circle represents the diffraction limit which is reached for almost any field.

cover a $9.54 \times 9.54 \text{ arcmin}^2$ with a scale of 0.56 as/px. The fore-optics have been then designed at magnification 1.

The optical layout of the spectrograph is reported in figure 9. The collimator is made of a pair of identical ZKN7-FPL53 separated doublets while the camera is made of two identical FPL53-ZKN7 separated doublets: the pairs differs one from the other. A SILICA window lens with identical curvature on both sides (easier mounting) closes the Apogee detector head.

The dispersion is obtained by insertion at the pupil location of an Amici Prism 66 mm long. The prism is made of Silica, BAF2 and CAF2 and it spreads the 0.45-0.95 μm wavelength range on 60 pixels, allowing the recording of 30 2-pixels bins along the range. The optical quality of ROSS is good as can be seen in the spot diagram reported in figure 10

By taking into account glass transmission and reflection (with suitable AR coating) the overall transmission of the camera (telescope, dichroic, CCD and AMICI prism not included) is estimated to be about 85%. An additional 2% loss should be expected from the telescope (silver coated), the minimum expected reflection of the dichroic (see above) is 88% and the AMICI is expected to uniformly lose about 2% at any wavelength. With the above numbers and the MARCONI CCD QE curve we computed the overall efficiency of ROSS; the curve is reported in figure 8.

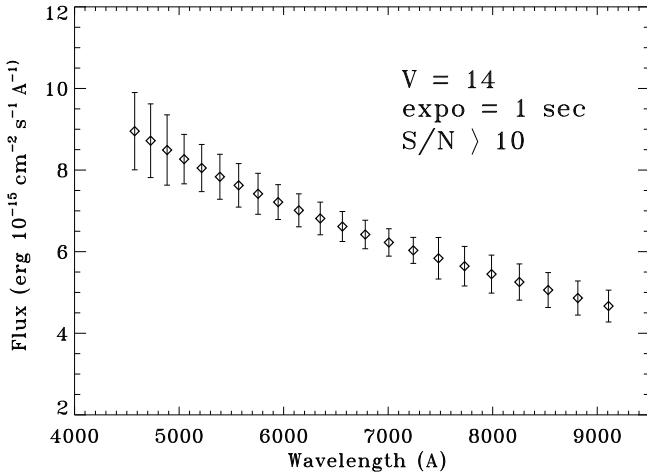


Fig. 11. Simulated spectrum of a magnitude $V=14$ GRB optical flash displaying a spectral slope $F_\lambda \propto \lambda^{-1.25}$. The exposure time is 1 second.

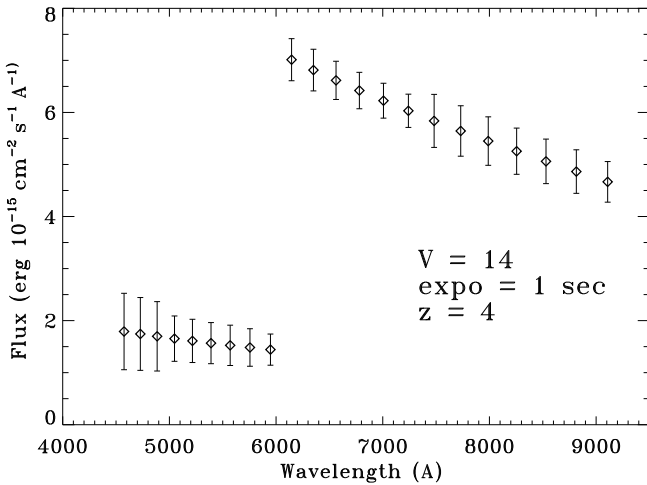


Fig. 12. Simulated spectrum of a magnitude $V=14$ GRB optical flash displaying a spectral slope $F_\lambda \propto \lambda^{-1.25}$ and a *Lyman* α dropout which falls in the optical range due to the high redshift (z) of the source. The exposure time is 1 second and the signal to noise ratio is about 4 below the break and greater than 10 above it.

In order to evaluate the expected performance of the ROSS spectrograph a simulated spectrum of a $V=14$ GRB optical flash with a spectral slope $F_\lambda \propto \lambda^{-1.25}$ was computed. The spectrum for a 1 sec exposure is shown in figure 11 where we can see that a $S/N > 10$ is reached at any wavelength.

By inserting a *Ly*- α drop due to high redshift of the source we obtain the spectrum shown in figure 12 where the S/N below the break is of about 4.

6. Site Location and Arrangements

A telescope like REM, specially because of the IR camera, has to be located in a dry and high altitude site with good weather conditions and a high percentage of observing nights. A viable and reliable connection to a large facility accepting Target of Opportunity alerts is in addition an important issue

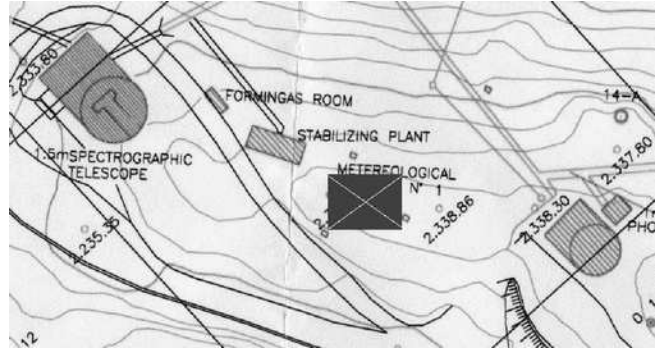


Fig. 13. The site where the REM observatory will be built, in between ESO 1.52 and ESO 1.0 telescopes at la Silla Observatory, Chile.

for the success of the project. For this reason we explored possible agreements with existing Observatories with a natural preference for the European Southern Observatory site at la Silla and Cerro Paranal, Chile.

An agreement to install REM at la Silla Observatory has been achieved in the framework of the FROST (Fast Robotic Observatory System for Transient), formed by REM and the French Project TAROT-S (see Boer et al, these proceedings). REM will be installed at la Silla Observatory at UTM (Zone 19) E 331,235 N 6,762,735 elev. 2,338.80 mt (see the exact location in the map in figure 13)

The observatory building is currently under construction. The Telescope will see the first light in October 2002.

References

- Akerlof C. & McKay T.A., 1999, IAUC 7100
- Cavallo G. & Rees M.J., 1978, MNRAS, 183, 359
- Costa E., et al., 1997, Nature, 387, 783
- Covino S. et al.: 1999, A&A, 348, L1
- Fossati G., Maraschi L., Celotti A., Comastri A., Ghisellini G., 1998, MNRAS, 299, 433
- Fruchter A.S., 1999, ApJ, 512, L1
- Ghisellini, G., Celotti, A., 1999, ApJ, 511, L93
- Ghisellini G., Celotti A., Fossati G., Maraschi L. & Comastri A., 1998, MNRAS, 301, 451
- Lazzati D., Ghisellini G., Celotti A. & Rees M.J., 2000, ApJ, 529, L17
- Liang E.P., 1997, ApJ, 491, L15
- Mészáros P., Rees M.J., 1993, ApJ, 405, 278
- Rees M.J., Mészáros P., 1992, MNRAS, 258, P41
- Rees M.J., Mészáros P., 1994, ApJ, 430, L93
- Sari R., Piran T.: 1997, MNRAS, 287, 110
- Sari R., Narayan R., Piran T., 1996, ApJ, 473, 204
- van Paradijs J., et al., 1997, Nature, 386, 686
- Wijers R.A.M.J. et al., 1999, ApJ, 523, L33
- Tanaka, Y., Shibazaki, N., 1996, ARA&A, 34, 607
- Filippenko A. et al., 1999, PASP, 111, 969
- McClintock J. et al., 2001, ApJ in press (astro-ph/0101421)
- Orosz J. et al., 2001, ApJ submitted (astro-ph/0103045)
- Della Valle M. et al., 1991, A&A 247, L33
- Rodonó, M., Houdebine, E.R., Catalano, S., et al 1989, in Solar and Stellar Flares, IAU Coll. 104,
- Rodonó M., 1990, in FlareStars in Stars Clusters, Association and Solar, IAU Symp 371.

- Rodonó, M., Cutispoto, G., 1988, in Activity in Cool Star Envelopes, O.Havnes et al (Eds.)
- Rol, E., Wijers, R.A.M.J., Vreeswik, P.M., et al , 2000, ApJ, 544, 707
- Becker, K., Morrison, P., 1974, ApJ, 187, L97.
- Grinin, V.P., 1976, Izv. Krym. Astrofiz. Obs. 60, 179
- Gurzadian, G.A., 1977, Ap. Space Sci. 52, 51
- Rodonó, M., Pucillo, M., Sedmak, G., De Biase, G.A., 1979, A&A, 76, 242
- Cristaldi, S., Gersheberg, R.E., Rodonó, M., 1980, A&A, 89, 123